

Magnetic Reconnection Controlled by Multi-Hierarchy Physics in an Open System

Ritoku HORIUCHI^{1,2)}, Shunsuke USAMI¹⁾, Hiroaki OHTANI^{1,2)} and Toseo MORITAKA³⁾

¹⁾*National Institute for Fusion Science, Toki 509-5292, Japan*

²⁾*The Graduate University for Advanced Studies, Toki 509-5292, Japan*

³⁾*Kobe University, Nada, Kobe 657-8501, Japan*

(Received 7 December 2009 / Accepted 12 March 2010)

Multi-hierarchy physics in magnetic reconnection is investigated using two kinds of numerical simulation models: the electromagnetic particle simulation model for an open system (PASMO) and the magnetohydrodynamic and particle-in-cell (MHD-PIC) interlocked model for the multi-hierarchy simulation of magnetic reconnection. A series of simulation studies using the PASMO code have disclosed that ion and electron dissipation regions form inside a kinetic regime in which ion and electron meandering orbit effects are crucial in triggering collisionless reconnection (CR). Anomalous resistivity leading to CR is also generated through the excitation of ion-ion kink instability in an ion-scale current sheet. We confirmed that the MHD-PIC interlocked model, based on the domain decomposition and multi-time-step methods, can describe collisionless driven reconnection in an open system as a multi-hierarchy phenomenon with high accuracy.

© 2010 The Japan Society of Plasma Science and Nuclear Fusion Research

Keywords: multi-hierarchy physics, magnetic reconnection, open system, anomalous resistivity, MHD-PIC interlocked model

DOI: 10.1585/pfr.5.S2006

1. Introduction

Magnetic reconnection is a typical cross-hierarchy phenomenon controlled by multi-hierarchy physics from microscopic electron dynamics to plasma transport on a macroscopic scale. A microscopic process leading to the generation of electrical resistivity, such as wave-particle interaction [1–7] and binary collisions, is needed to excite magnetic reconnection. On the other hand, global plasma transport and global changes in field topology occur as a result of magnetic reconnection [8]. Note that these physical processes are not independent but are strongly coupled in a complex way, making magnetic reconnection phenomena more complex. Thus, many problems remain unsolved despite a long history of magnetic reconnection studies. For example, particle simulations using the PASMO code [9–13] have demonstrated that dynamical magnetic reconnection behavior changes from steady to intermittent state if the spatial scale of plasma inflow into the reconnection region increases over some critical value. Furthermore, in steady reconnection, the reconnection electric field generated by microscopic physics evolves so as to balance the flux inflow rate at the inflow boundary, which is controlled by macroscopic physics. These results suggest that microscopic physics in the reconnection region depends strongly on external macroscopic physics. Thus, the entire picture of magnetic reconnection should be clarified by solving both microscopic and macroscopic physics, consistently and simultaneously.

A number of theoretical and numerical simulation studies have disclosed two triggering mechanisms that break the frozen-in condition and excite magnetic reconnection in a collisionless plasma. One is due to the anomalous resistivity associated with plasma instabilities [1–7], and the other is due to microscopic kinetic effects of particles with finite mass and finite orbit amplitude [9–16]. In Section 2, we discuss the triggering mechanisms associated with various microscopic physics using the PASMO code, in which information from macroscopic physics is introduced into a microscopic system as boundary conditions.

To clarify the entire picture of magnetic reconnection, we recently developed the MHD-PIC interlocked model for multi-hierarchy simulation of magnetic reconnection based on the domain decomposition method and a multi-time-step scheme [17–19]. This model has three parts: an MHD model to describe the global dynamics of reconnection phenomena, an electromagnetic PIC model to describe microscopic processes near the reconnection point, and an interface model to describe the interaction between the micro and macro hierarchies. In Section 3, we give an overview of the MHD-PIC interlocked model and its application to collisionless driven reconnection.

author's e-mail: horiuchi.ritoku@nifs.ac.jp

2. Microscopic Triggering Mechanisms for Collisionless Reconnection

There are several hot issues in the microscopic triggering mechanism for collisionless reconnection (CR). The first is whether ion or electron dynamics dominate CR. The second is whether the inertia effect or finite orbit effect is the dominant mechanism. The third is the relationship between the anomalous resistivity due to wave-particle interaction and particle kinetic effects in CR. To answer these questions, we carried out a series of particle simulations in open systems using the PASMO code [9–13]. The initial condition used for these simulations is one-dimensional equilibrium with a Harris-type antiparallel magnetic field configuration along the x -axis.

$$B_x(y) = B_0 \tanh(y/L), \quad (1)$$

where B_0 is a constant and L is the scale height along the y -axis. A magnetically neutral sheet exists at $y = 0$ in the initial equilibrium. The initial particle distribution is assumed to be a shifted Maxwellian with spatially constant temperature and an average particle velocity equal to the diamagnetic drift velocity. The physical quantities are normalized by the light velocity c and the electron gyration frequency ω_{ce} , for example, velocity $v = \tilde{v}c$, time $t = \tilde{t}\omega_{ce}^{-1}$, and spatial scale $x = \tilde{x}c/\omega_{ce}$, unless stated.

2.1 Mechanism of generation of anomalous resistivity in an ion-scale current sheet

A three-dimensional particle simulation study [3] revealed that two kinds of plasma instabilities are excited in an ion-scale current sheet with no external driving source. First, the lower hybrid drift instability (LHDI) [1] is observed to grow in the periphery of the current sheet. The lower hybrid drift mode, however, does not penetrate into the central high- β region of the current sheet because it undergoes strong damping there. Thus, it cannot be a direct cause of anomalous resistivity at the neutral sheet. This result is consistent with theory [1] and satellite observations [20]. Later, a drift kink instability (DKI) [2–4, 21] is triggered at the neutral sheet as a result of nonlinear deformation of the current sheet by the LHDI. The reconnection electric field grows at the neutral sheet in accordance with the excitation of the DKI. On the other hand, theoretical linear analysis [4] has suggested that the growth rate of the DKI decreases with the mass ratio, and becomes negligibly small for a real mass ratio.

To clarify the physical reason for the discrepancy between simulations and linear analysis, Moritaka and Horiuchi [6, 7] performed a series of two-dimensional particle simulations for various mass ratios. Figure 1 shows the mass ratio dependence of the growth rate of kink modes, where the electron mass changes while the ion mass is fixed. The DKI is split into two modes with different wavelengths for a large mass ratio of $m_i/m_e > 100$, i.e., a longer kink mode of $kL \approx 0.5$ and a shorter kink mode of

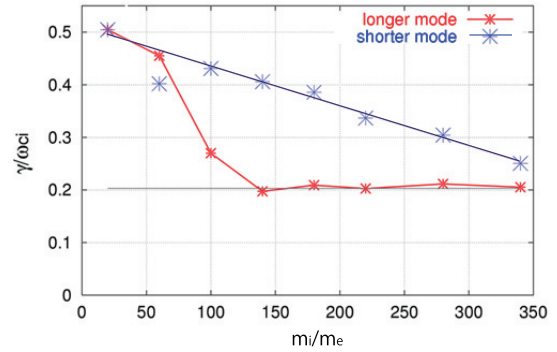


Fig. 1 Mass ratio dependence of the growth rate of the shorter (blue) and longer (red) kink modes; the electron mass changes, while the ion mass is fixed [7].

$kL \approx 1.7$, where k is a typical wavenumber. Note that the longer kink mode maintains a constant growth rate ($\gamma/\omega_{ci} \approx 0.2$) even for a large mass ratio, while the rate decreases with mass ratio for the shorter kink mode.

A detailed analysis of simulation data [7] has disclosed the following physical mechanism in the longer kink mode. The ion distribution is modified through an interaction between electrostatic fluctuation excited by the LHDI in the periphery and meandering ions with large orbit amplitude in the ion-scale current sheet. In this process, another peak is generated around the origin of velocity space ($v = 0$) in addition to the initial shifted Maxwellian distribution, and thus the distribution changes to a two-component profile. The relative motion between the two ion components causes the growth of the longer kink mode, called the ion-ion kink mode, in the central region of the current sheet [4]. Therefore, the longer kink mode is almost independent of electron mass, and it is expected to maintain a finite growth rate for a real mass ratio. The anomalous resistivity generated in this process, which is defined by the ratio of the electric field to the current density, is estimated to be about 0.1 of the Hall resistivity [6, 12]. This result is consistent with previous simulations [6, 12]. The generated electric field results in the penetration of magnetic flux into the dissipation region with a velocity nearly equal to that of the $\mathbf{E} \times \mathbf{B}$ drift associated with the generated electric field. The temporal evolution of the normalized reconnection rate is plotted in Fig. 2, where the normalized reconnection rate R_{rec} is defined by the penetration velocity into the ion dissipation region divided by the Alfvén velocity upstream. The reconnection rate is in the range of $R_{\text{rec}} \approx 0.01$ -0.1, which is large enough to explain the magnetic reconnection phenomena observed in the magnetosphere [22] and laboratory experiments [23].

2.2 Two-scale structure of a kinetic regime

Under the influence of an external driving flow, the system evolves into a quasi-steady state after an initial transient phase if the driving flow satisfies some condi-

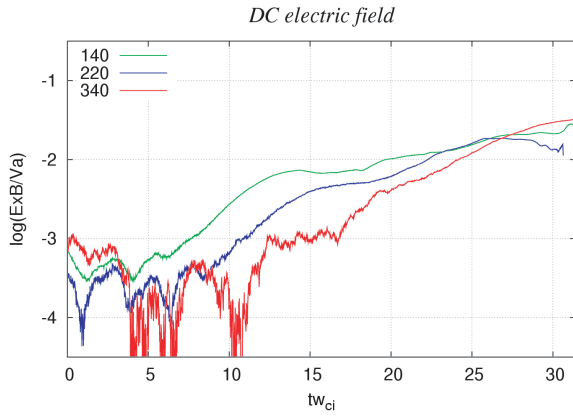


Fig. 2 Temporal evolution of normalized reconnection rate for mass ratio $m_i/m_e = 140$ (green), 220 (blue), and 340 (red); the electron mass changes, while the ion mass is fixed.

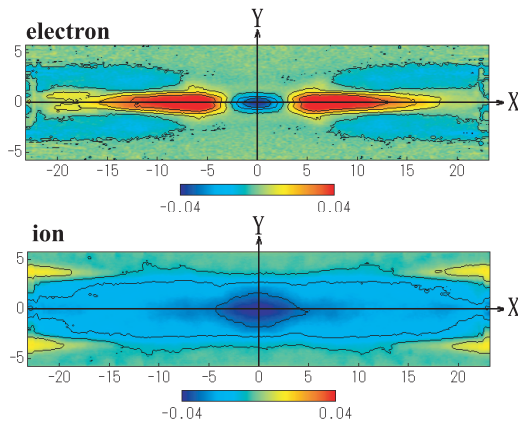


Fig. 3 Spatial profiles of the z -components of $\mathbf{E} + \mathbf{v}_e \times \mathbf{B}$ (top) and $\mathbf{E} + \mathbf{v}_i \times \mathbf{B}$ (bottom) in the (x, y) plane at $\omega_{ce} t = 1023$; red and blue colors indicate positive and negative values, respectively.

tion [9]. A kinetic regime appears in the central current sheet in the quasi-steady state, where microscopic kinetic effects become dominant. Figure 3 demonstrates a typical three-dimensional particle simulation result for the ion-to-electron temperature ratio $T_i/T_e = 1$, $m_i/m_e = 50$, $\omega_{pe}/\omega_{ce} = 2.5$, and $E_d = -0.04B_0$, where E_d is the driving electric field imposed at the upstream boundary. Spatial profiles of the z -components of $\mathbf{E} + \mathbf{v}_e \times \mathbf{B}$ (top) and $\mathbf{E} + \mathbf{v}_i \times \mathbf{B}$ (bottom) are plotted at the quasi-steady state ($\omega_{ce} t = 1023$), where \mathbf{v}_i and \mathbf{v}_e are the ion and electron fluid velocities, respectively. The kinetic regime clearly consists of two dissipation regions with different spatial scales, where the frozen-in condition $\mathbf{E} + \mathbf{v}_j \times \mathbf{B} = 0$ ($j = i, e$) is broken: an outer ion dissipation region (IDR) and an inner electron dissipation region (EDR) [9, 24, 25].

What mechanism determines the spatial scales of these two dissipation regions? Considering the violation mechanism of the frozen-in condition, it is useful to exam-

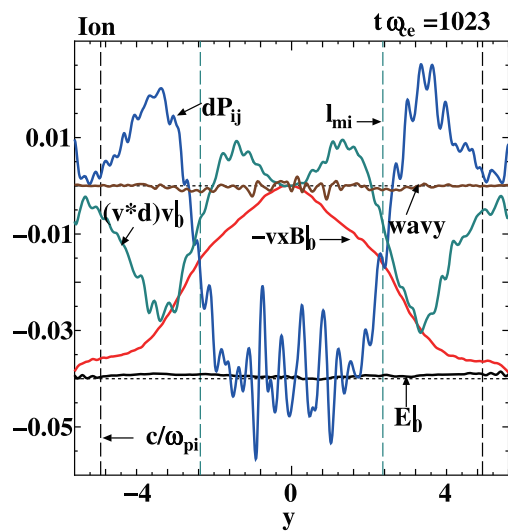
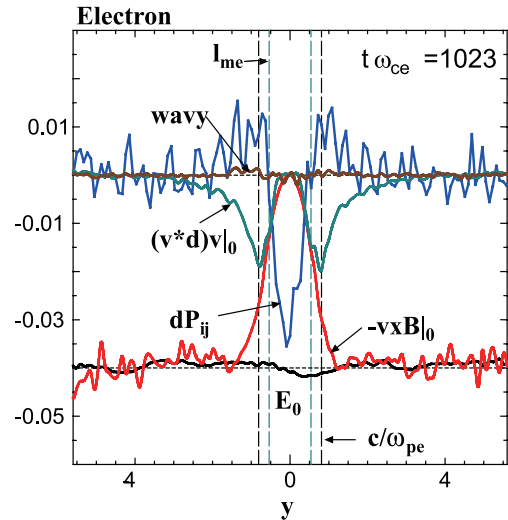


Fig. 4 Spatial profiles of non-ideal terms for electrons (top) and ions (bottom) along the y -axis at $\omega_{ce} t = 1023$; the subscript 0 denotes the DC component, and the curve labeled “wavy” represents the summation of wavy components.

ine non-ideal terms in two-fluid equations such as

$$n_j q_j (\mathbf{E} + \mathbf{v}_j \times \mathbf{B}) = m_j n_j \left(\frac{\partial}{\partial t} + \mathbf{v}_j \cdot \nabla \right) \mathbf{v}_j + \frac{\partial \bar{\mathbf{P}}_j}{\partial x}, \quad (2)$$

where the subscript j ($= i, e$) denotes ions or electrons, and $\bar{\mathbf{P}}_j$ is the pressure tensor. Spatial profiles of the z -component of non-ideal terms for electrons (top) and ions (bottom) along the y -axis are plotted in Fig. 4. All the field quantities are expanded into a DC and a fluctuating component to distinguish the effect of plasma instabilities from the particle kinetic effect. The effect of plasma instabilities is negligibly small in the steady state (brown curves). The z -component of the electric field becomes uniform in the steady state (solid black curve); that is, the input rate of magnetic flux at the upstream boundary is balanced with the reconnection rate. The pressure tensor term (blue

curve) becomes dominant within the particle meandering scale (l_{mi} or l_{me}) near the reconnection point ($y = 0$) for both electrons and ions. The particle meandering scale is given by the distance that satisfies the condition

$$\rho(y) = y, \quad (3)$$

where $\rho(y)$ is the local Larmor radius at a distance y from the neutral sheet [11]. This result is deeply connected to the fact that the off-diagonal components of pressure tensor terms originate from the non-gyrotropic motion near the neutral sheet, so-called ‘‘meandering motion.’’ On the other hand, the inertia term (green curve) grows in the two-fluid region of $c/\omega_{pj} > y > l_{mj}$ ($j = i, e$), but it is almost canceled by the pressure tensor term with an opposite sign [24]. Thus, the spatial size for the violation of the frozen-in condition is roughly given by the particle meandering scale (l_{mi} or l_{me}). These results are consistent with those of the previous simulations [9–11, 15, 24]. When charged particles move into the meandering region, they are free from the frozen-in constraint, and particles with different origins mix. In other words, meandering motion of charged particles can be a microscopic cause of electrical resistivity, leading to the excitation of CR.

2.3 Particle kinetic effect and plasma instabilities

In the previous subsections, we discussed two triggering mechanisms for CR separately. In a real system, however, both these mechanisms exist simultaneously. Here, let us examine the relationship between the microscopic particle kinetic effect and the anomalous resistivity associated with the kink mode. Three-dimensional simulations in an open system [3, 17] have demonstrated that CR is first triggered by the meandering orbit effect and then the system relaxes into the quasi-steady state. The DKI gradually grows in the EDR in the intermediate quasi-steady state and changes the plasma profiles significantly there. Figure 5 illustrates the spatial profiles of various terms in the electron force balance equation at $\omega_{ce}t = 1293$, where the curve labeled ‘‘wavy’’ represents the summation of the wavy components. The electron pressure tensor term decreases, whereas the nonlinear wave coupling term increases at the center of the EDR and expands toward the IDR as the DKI grows.

Figure 6 shows the spatial profiles of the dominant off-diagonal component of electron pressure tensor P_{eyz} (top-left), the z -components of the nonlinear wave coupling term $v_{e1} \times \mathbf{B}_1$ (top-right) and $\mathbf{E} + v_e \times \mathbf{B}$ (bottom-left), and B_x/T_e (bottom-right) at $\omega_{ce}t = 1293$, where the profiles are plotted on the (y, z) plane, including the mid-point $(x, y, z) = (0, 0, 0)$. The DKI modifies the P_{eyz} profile so as to decrease the DC component and increase the wavy component (top-left). Thus, the electron pressure tensor term averaged along the z -axis decreases as the DKI grows. The DC component is generated in the nonlinear wave-particle coupling term to compensate for the decrease in

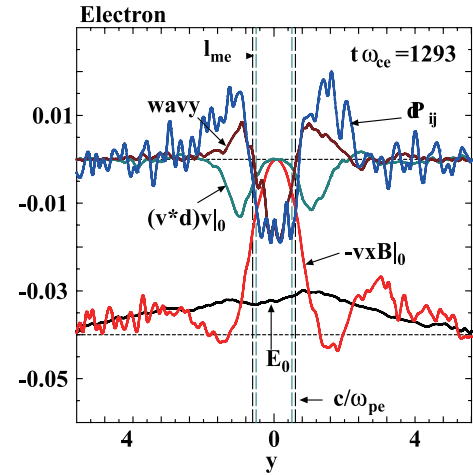


Fig. 5 Spatial profiles of non-ideal terms for electrons along the y -axis at $\omega_{ce}t = 1293$.

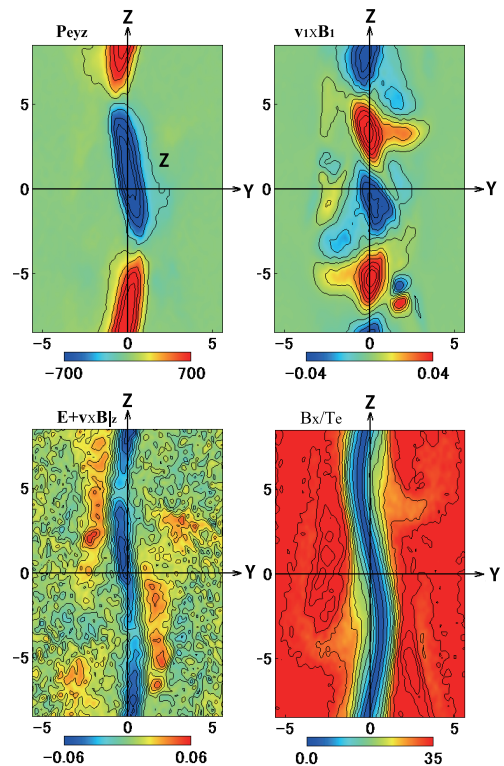


Fig. 6 Spatial profiles of off-diagonal component of electron pressure tensor P_{eyz} (top-left), the z -components of nonlinear wave coupling term $v_{e1} \times \mathbf{B}_1$ (top-right) and $\mathbf{E} + v_e \times \mathbf{B}$ (bottom-left), and B_x/T_e (bottom-right) in the (y, z) plane at $\omega_{ce}t = 1293$.

the electron pressure tensor term through phase mismatch between the plasma disturbed motion and electromagnetic (EM) fluctuation in the kinetic regime (top-right) [6]. Energy conversion from the EM field to particles occurs in the kinetic regime. We discuss this process by examining the behavior of the magnetic moment, $\mu = mv_{\perp}^2/2B$ (v_{\perp} is the particle velocity perpendicular to the magnetic field),

which is an adiabatic constant in an ideal MHD plasma. The ensemble average of μ over the particles with temperature T is given by $\langle \mu \rangle = m \langle v_{\perp}^2 \rangle / 2B \propto T/B$. As shown at the bottom-right and bottom-left panels of Fig. 6, the average $\langle \mu \rangle$ increases in the EDR where the electron frozen-in condition is broken. This indicates that considerable energy conversion from the EM field to electrons occurs in the EDR. Furthermore, the growth of the DKI enhances the conversion and widens the conversion region.

3. Multi-Hierarchy Simulation of Magnetic Reconnection

The microscopic triggering mechanism for CR has been investigated using the PASMO code in which information on the macroscopic system is introduced as boundary conditions. As a result, the microscopic reconnection mechanism and its dynamic behavior in an open system are found to be strongly dependent on the conditions of the external driving source, such as the flux inflow rate and its spatial profile [9–11]. To obtain important information for constructing a multi-hierarchy model of magnetic reconnection, using a three-dimensional particle simulation we examine how the ion distribution function behaves in collisionless driven systems [16]. Figure 7 illustrates the ion distribution function in the phase space (y, v_y) at $\omega_{ce}t = 1023$; the left and right boundaries correspond to the inflow boundaries, and a reconnection point is located at the center of the y -axis. The ion distribution function remains shifted Maxwellian outside the IDR ($y > l_{mi}$). In contrast, the ion distribution function differs considerably from the shifted Maxwellian in the IDR. In other words, we need a precise description of particle dynamics near the reconnection point, where the Larmor radius is much larger than the typical spatial scale of the background plasma, whereas the MHD approximation holds in the region far from the reconnection point.

Using these characteristic features of magnetic reconnection, we have developed the MHD-PIC interlocked model, which relies on the domain decomposition and

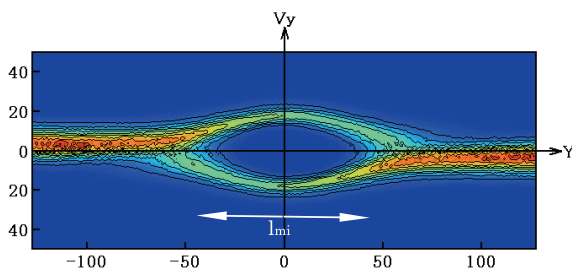


Fig. 7 Ion distribution function in the phase space (y, v_y) at $\omega_{ce}t = 1023$; profile is obtained from a three-dimensional particle simulation using the PASMO code. Left and right boundaries of the y -axis correspond to the inflow boundaries; the y and v_y axes are normalized by the Debye length and $0.3v_{ti}$ (v_{ti} : ion thermal velocity), respectively.

multi-time-step methods [18, 19, 26]. The PIC model (PASMO code) is adopted to describe microscopic kinetic dynamics of magnetic reconnection near the reconnection point. An MHD model [27] describes the global dynamics in the region far from the reconnection point. To interlock the two models smoothly, we insert an interface domain between the PIC and MHD domains and adopt a hand-shake scheme there [28]. The interface domain is located in the region where the ion distribution function can be described by the shifted Maxwellian, so both the PIC and MHD models are applicable (see Fig. 7). The physical quantities in the interface domain are connected smoothly by the following interpolation scheme [26] as

$$Q = \alpha(y)Q_{\text{MHD}} + (1 - \alpha(y))Q_{\text{PIC}}, \quad (4)$$

where the interpolation function $\alpha(y)$ changes from 0 to 1 according to the spatial position y . Q_{MHD} and Q_{PIC} are the field quantities obtained from the MHD and PIC simulations, respectively.

First, as a numerical check, we applied the developed interlocked model to the propagation of a one-dimensional linear Alfvén wave in a simplified geometry [18, 19]. The Alfvén wave was found to propagate smoothly from the MHD domain to the PIC domain and vice versa, except for small fluctuations in the PIC region. This confirms that the present interlocked model works well. Next, we applied it to collisionless driven reconnection in a two-dimensional open system assuming that the MHD domains are connected with the PIC domain only in the upstream region, and physical quantities are periodic at the downstream boundary [19]. Plasma is supplied to the system through the upstream boundary of the MHD domains by the $\mathbf{E} \times \mathbf{B}$ drift motion. The driving electric field imposed at the upstream boundary is programmed to evolve from zero to the constant value, $E_0 (= -0.04B_0)$, with a spatially uniform shape. The current sheet evolves because of the accumulation of magnetic flux by the driving field and the CR sets at the center of the current sheet. Figure 8 demonstrates the spatial profiles of magnetic field lines (top) and vector plots of fluid velocity (bottom) in the (x, y) plane at $\omega_{ce}t = 1485$, where $m_i/m_e = 100$, $l_{mi} \approx 5c/\omega_{ce}$ and $c/\omega_{pi} \approx 13c/\omega_{ce}$. Clearly, both plasma and magnetic flux are smoothly supplied to the PIC domain ($|y/(c/\omega_{ce})| < 21.875$) through the interface domain (light blue for $21.875 < |y/(c/\omega_{ce})| < 23.875$) from the MHD domain (yellow for $23.875 < |y/(c/\omega_{ce})| < 29.875$).

Let us examine the physical reliability by comparing the results of the multi-hierarchy and the PASMO simulations (see Fig. 4). Figure 9 shows the spatial profiles of non-ideal terms in the ion force balance equation along the y axis at $\omega_{ce}t = 1485$ for the same case as Fig. 8. The ion pressure tensor term (green curve) becomes dominant within the ion meandering scale ($|y| < l_{mi}$); the inertia term (red curve) grows in the two-fluid region of $c/\omega_{pi} > |y| > l_{mi}$, but it is canceled by the pressure tensor term with the opposite sign. These results are con-

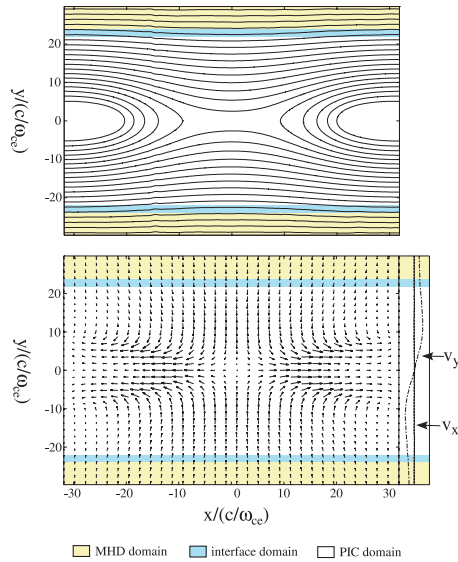


Fig. 8 Spatial profiles of magnetic field lines (top) and vector plots of fluid velocity (bottom) in the (x, y) plane at $\omega_{ce}t = 1485$, where $m_i/m_e = 100$, $l_{mi} \approx 5c/\omega_{ce}$ and $c/\omega_{pi} \approx 13c/\omega_{ce}$. Velocity components v_x and v_y along the y -axis passing the reconnection point are plotted on the right side of the bottom panel.

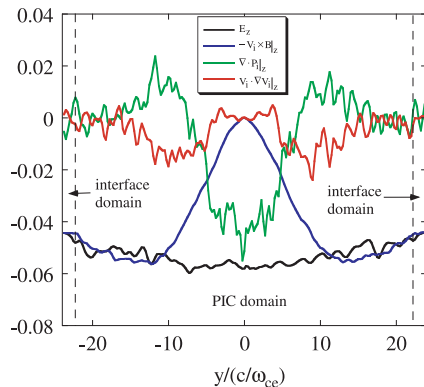


Fig. 9 Spatial profiles of non-ideal terms in the z -component of the ion force balance equation along the y -axis at $\omega_{ce}t = 1485$ for the same case as Fig. 8.

sistent with those obtained from the PASMO simulations [9–11, 24]. Thus, the present MHD-PIC interlocked model can describe collisionless driven reconnection in an open system as a multi-hierarchy phenomenon with high accuracy.

4. Summary

We investigated multi-hierarchy physics in magnetic reconnection by means of electromagnetic particle simulation and MHD-PIC interlocked simulation. Two microscopic triggering mechanisms exist in CR. Electromagnetic PIC simulations using the PASMO code have disclosed that two dissipation regions with different spatial scales form inside the kinetic regime, and both electron

and ion meandering orbit effects are crucial in triggering CR. Furthermore, anomalous resistivity is also generated through excitation of ion-ion kink instability in an ion-scale current sheet at the late phase of the simulation; it enhances the process of energy conversion from the EM field to particles in collisionless plasmas.

We developed the MHD-PIC interlocked simulation model based on the domain decomposition and multi-time-step methods for investigating multi-hierarchy physics in magnetic reconnection. By comparing our results with PASMO simulation results we confirmed that the developed MHD-PIC interlocked model can describe collisionless driven reconnection in an open system as a multi-hierarchy phenomenon with high accuracy. We now plan to extend the interlocked model and apply it to various reconnection phenomena.

This work was partially supported by the Research Cooperation Program on “Hierarchy and Holism in Natural Sciences 2” at the National Institutes of Natural Sciences, and by the General Coordinated Research program at the National Institute for Fusion Science (NIFS08KTAN005, NIFS08KNXN121).

- [1] N. A. Krall and P. C. Liewer, *Phys. Rev.* **4**, 2094 (1971).
- [2] Z. Zhu and R. M. Winglee, *J. Geophys. Res.* **101**, 4885 (1996).
- [3] R. Horiuchi and T. Sato, *Phys. Plasmas* **6**, 4565 (1999).
- [4] W. Daughton, *Phys. Plasmas* **6**, 1329 (1999).
- [5] W. Daughton, G. Lapenta and P. Ricci, *Phys. Rev. Lett.* **93**, 105004 (2004).
- [6] T. Moritaka, R. Horiuchi and H. Ohtani, *Phys. Plasmas* **14**, 102109 (2007).
- [7] T. Moritaka and R. Horiuchi, *Phys. Plasmas* **15**, 092114 (2008).
- [8] J. Li, T. Sato and A. Kageyama, *Science* **295**, 1887 (2002).
- [9] W. Pei, R. Horiuchi and T. Sato, *Phys. Plasmas* **8**, 3251 (2001).
- [10] W. Pei, R. Horiuchi and T. Sato, *Phys. Rev. Lett.* **87**, 235003 (2001).
- [11] R. Horiuchi and T. Sato, *Phys. Plasmas* **1**, 3587 (1994).
- [12] R. Horiuchi and T. Sato, *Phys. Plasmas* **4**, 277 (1996).
- [13] H. Ohtani and R. Horiuchi, *Plasma Fusion Res.* **4**, 024 (2009).
- [14] D. Biskamp, *Magnetic Reconnection in Plasmas* (Cambridge University Press, Cambridge, 2000).
- [15] M. Hesse, K. Schindler, J. Birn and M. Kuznetsova, *Phys. Plasmas* **6**, 1781 (1999).
- [16] R. Horiuchi and H. Ohtani, *Comm. Comp. Phys.* **4**, 496 (2008).
- [17] R. Horiuchi, H. Ohtani and A. Ishizawa, *J. Plasma Phys.* **72**, 953 (2006).
- [18] S. Usami, H. Ohtani, R. Horiuchi and M. Den, *Comm. Comp. Phys.* **4**, 537 (2008).
- [19] S. Usami, H. Ohtani, R. Horiuchi and M. Den, *Plasma Fusion Res.* **4**, 049 (2009).
- [20] S. D. Bale, F. S. Mozer and T. Phan, *Geophys. Res. Lett.* **29**, 2180 (2002).
- [21] D. Winske, *Phys. Fluids* **24**, 1069 (1981).
- [22] F. S. Mozer, T. Phan and S. D. Bale, *Phys. Rev. Lett.* **89**, 015002 (2002).

- [23] M. Yamada, Phys. Plasma **14**, 058102 (2007).
- [24] A. Ishizawa and R. Horiuchi, Phys. Rev. Lett. **95**, 045003 (2005).
- [25] M. A. Shay, J. F. Drake, B. N. Rogers and R. E. Denton, J. Geophys. Res. **106**, 3759 (2001).
- [26] R. Horiuchi, S. Usami, H. Ohtani and M. Den, Plasma Fusion Res. **4**, 184 (2009).
- [27] R. Horiuchi and T. Sato, Phys. Fluids **B1**, 581 (1989).
- [28] T. Sugiyama and K. Kusano, J. Comput. Phys. **227**, 1340 (2007).